

Reduced SNAP-25 increases PSD-95 mobility and impairs spine morphogenesis

G Fossati^{1,2}, R Morini^{1,2}, I Corradini^{1,3}, F Antonucci^{1,3}, P Trepte⁴, E Edry⁵, V Sharma⁵, A Papale⁶, D Pozzi², P Defilippi⁷, JC Meier^{8,9}, R Brambilla⁶, E Turco⁷, K Rosenblum⁵, EE Wanker⁴, NE Ziv¹⁰, E Menna^{*2,3} and M Matteoli^{1,2}

Impairment of synaptic function can lead to neuropsychiatric disorders collectively referred to as synaptopathies. The SNARE protein SNAP-25 is implicated in several brain pathologies and, indeed, brain areas of psychiatric patients often display reduced SNAP-25 expression. It has been recently found that acute downregulation of SNAP-25 in brain slices impairs long-term potentiation; however, the processes through which this occurs are still poorly defined. We show that *in vivo* acute downregulation of SNAP-25 in CA1 hippocampal region affects spine number. Consistently, hippocampal neurons from SNAP-25 heterozygous mice show reduced densities of dendritic spines and defective PSD-95 dynamics. Finally, we show that, in brain, SNAP-25 is part of a molecular complex including PSD-95 and p140Cap, with p140Cap being capable to bind to both SNAP-25 and PSD-95. These data demonstrate an unexpected role of SNAP-25 in controlling PSD-95 clustering and open the possibility that genetic reductions of the protein levels – as occurring in schizophrenia – may contribute to the pathology through an effect on postsynaptic function and plasticity.

Cell Death and Differentiation (2015) 22, 1425–1436; doi:10.1038/cdd.2014.227; published online 13 February 2015

Synapses are complex cellular junctions specialized for communication between neurons. Epidemiological and genetic studies demonstrated that deficiencies in synapse function¹ are implicated in a wide range of brain disorders, including neurodegenerative² and psychiatric diseases such as schizophrenia^{3,4} and autism.^{5,6} A hallmark of synaptic specializations is their dependence on highly organized complexes of proteins that interact with each other. Therefore, the loss or modification of key synaptic proteins might directly affect the properties of such networks and, ultimately, synaptic function.

SNAP-25 is a component of the SNARE complex, which is central to synaptic vesicle exocytosis^{7,8} and which has a role in the regulation of voltage-gated calcium channels.^{9,10} The *SNAP25* gene has been associated with attention deficit hyperactivity disorder (ADHD)^{11,12} and with schizophrenia.^{13,14} Consistently, SNAP-25 levels are lower in the hippocampus¹⁵ and in the frontal lobe¹⁶ of patients with schizophrenia. DNA

variants of the *SNAP25* gene that associate with ADHD are also associated with reduced expression level of the transcript in prefrontal cortex.¹⁷ Finally, reduction of SNAP-25 levels has been found to cause neurodegeneration in mice lacking the synaptic vesicle protein Cysteine-string protein- α , possibly due to the impaired SNARE-complex assembly produced by the decreased SNAP-25.¹⁸ The mechanisms by which reduced SNAP-25 expression may result in a psychiatric disease are still undefined, although alterations in neurotransmitter release have been indicated as potential causative processes.^{19,20}

Recently an unexpected postsynaptic role of SNAP-25 has been described, with the protein controlling NMDA and kainate receptor trafficking.²¹ Furthermore, it has been lately found that acute SNAP-25 downregulation results in LTP impairment^{21,22} and that acute reduction of the protein affects spine morphogenesis *in vitro*, through a process involving the protein p140Cap.²³ These data, together with the evidence of

¹Department of Biotechnology and Translational Medicine, University of Milan, Milano 20129, Italy; ²Humanitas Clinical and Research Center, Laboratory of Pharmacology and Brain Pathology, Via Manzoni 56, Rozzano, 20089 Milano, Italy; ³Istituto di Neuroscienze del CNR, Milano 20129, Italy; ⁴Neuroproteomics, Max Delbrueck Center for Molecular Medicine (MDC), Berlin 13125, Germany; ⁵Sagol Department of Neurobiology, Center for Gene Manipulation in the Adult Brain (CGMB), Haifa University, Haifa, Israel; ⁶Division of Neuroscience, Institute of Experimental Neurology, San Raffaele Scientific Institute and University, Milano 20132, Italy; ⁷Department of Molecular Biotechnology and Health Sciences, University of Torino, Torino 10124, Italy; ⁸RNA Editing and Hyperexcitability Disorders Helmholtz Group, Max Delbrück Center for Molecular Medicine, Berlin, Germany; ⁹TU Braunschweig, Zoological Institute, Division of Cell Biology and Cell Physiology, Braunschweig, Germany and ¹⁰Network Biology Labs and Faculty of Medicine, Technion, 33000 Haifa, Israel

*Corresponding authors: E Menna, CNR Institute of Neuroscience, Via Vanvitelli 32, 20129 Milano, Italy. Tel: +39 0250317095; Fax: +39 0250317132; E-mail: e.menna@in.cnr.it or M Matteoli, Department of Medical Biotechnology and Translational Medicine, University of Milan, Via Vanvitelli 32, 20129 Milano, Italy. Tel: +39 250317095; Fax: +39 0250317132; E-mail: michela.matteoli@unimi.it

Abbreviations: ADHD, attention deficit hyperactive disorder; AMPA, α -Amino-3-hydroxy-5-methyl-4-isoxazolepropionic acid; AraC, cytosine arabinoside; BotT/E, Botulinum toxin type E; BSA, bovine serum albumine; Bsn, Bassoon; CA1, Cornus Ammonis 1; CTA, conditioned taste aversion; DIV, days *in vitro*; DTT, Dithiothreitol; EDTA, Ethylenediaminetetraacetic acid; EGTA, ethylene glycol tetraacetic acid; FACS, fluorescence activated cell sorting; FRAP, fluorescence recovery after photobleaching; GAPDH, glyceraldehyde 3-phosphate dehydrogenase; GFP, green fluorescent protein; HEK293, Human Embryonic Kidney 293; HEPES, (2-hydroxyethyl)-1-piperazineethanesulfonic acid; Het, heterozygous; KRH, Krebs' Ringer's-HEPES; LTD, long-term depression; LTP, long-term potentiation; LUMIER, Luminescence-based Mammalian interActome; mEPSC, miniature excitatory postsynaptic current; NMDA, *N*-Methyl-D-aspartic acid or *N*-Methyl-D-aspartate; NR1, NMDA receptor subunit 1; PBS, phosphate-buffered saline; PFA, paraformaldehyde; PI, propidium iodide; PLA, proximity ligation assay; PMSF, phenylmethanesulfonyl fluoride; PSD-95, postsynaptic density of 95 kDa; RFP, red fluorescent protein; shRNA, short hairpin RNA; siRNA, small interference RNA; SNAP-25, synaptosomal-associated protein 25; SNARE, Soluble NSF Attachment Protein REceptor; SRCIN1, SRC kinase signaling inhibitor 1; SV2A, synaptic vesicle 2A; Wt, wild type

Received 10.3.14; revised 22.10.14; accepted 26.11.14; Edited by G Melino; published online 13.2.15

a role for SNAP-25 in human intellectual disability,²⁴ open the possibility that besides a presynaptic impact, chronic reductions of SNAP-25 levels, as described in the hippocampus of schizophrenic patients, may impair the structure and/or function of the postsynaptic compartment. If confirmed, this possibility, which has never been addressed before, would provide a logical frame for the protein involvement in different psychiatric diseases, characterized by defective formation and function of the postsynaptic compartment.

In this study, we demonstrate that a genetic, partial reduction of the protein levels, as occurring in psychiatric diseases, results in a flawed maturation of postsynaptic specializations, reduced densities of dendritic spines, impaired synaptic potentiation, and PSD-95 destabilization.

Results

Acute reduction of SNAP-25 expression in mice hippocampus alters spine morphology. We used a lentiviral approach to induce *in vivo* silencing of SNAP-25 by expressing short hairpin RNA specific for SNAP-25 (SNAP-25-shRNA) or scrambled shRNA together with eGFP (Supplementary Figure S1A). We validated SNAP-25 knock-down in mouse primary neuronal cultures by real-time PCR analysis (Supplementary Figure S1B). To functionally confirm *in vivo* the SNAP-25 shRNA efficacy, we took advantage of the previous demonstration that SNAP-25 heterozygous mice show defective conditioned test aversion (CTA) memory²⁵ and that SNAP-25 immunoreactivity increases in the gustatory cortices in response to food and chemical stimulation.²⁶ We then used CTA as a paradigm test to provide the functional demonstration that acute downregulation of SNAP-25 is effective and induces the same behavioral defects already described in transgenic mice.²⁵ We therefore injected the indicated vectors into the gustatory cortex, which resides within the insular cortex, and CTA memory was tested 7 days after. The scrambled-injected rats displayed normal CTA²⁷ while SNAP-25 shRNA-injected rats were impaired (Supplementary Figure S1C), thus indicating that acute reduction of the protein recapitulates the functional defects already shown in SNAP-25 heterozygous mice.

It has been recently shown that postsynaptic SNAP-25 regulates surface NMDAR levels and has a role in LTP induction in the CA1 hippocampal neurons.²² Given that activity-driven changes of synaptic efficacy underlying hippocampal LTP require proper dendritic spine morphogenesis, we quantified by confocal microscopy spine density and morphology of CA1 neurons positive for the fluorescent reporter eGFP upon injection of the SNAP-25 shRNA or the scramble vectors. Mice were perfused 15 days after lentiviral vector injection and the brains were sectioned and immunostained for GFP (Figure 1a, low magnification images). Spine density and morphology was analyzed on secondary and tertiary branches of apical dendrites in the stratum radiatum (SR; Figure 1a, high magnification images). SNAP-25 knockdown causes a significant decrease in spine density on CA1 dendrites with respect to controls (Figure 1b). Such a decrease was accompanied by a reduction in the number of mushroom spines and an increase in the number of thin spines

(Figure 1c). Adult Het mice show similar but minor defects in spine density and morphology (Supplementary Figure S1D and E), probably due to the higher protein level²⁵ in the adult Het animals with respect to the SNAP-25 shRNA injected hippocampi.

Defective postsynaptic maturation of glutamatergic synapses in SNAP-25 heterozygous cultures. To investigate whether reduced SNAP-25 expression impairs the proper postsynaptic maturation of glutamatergic synapses, we used primary hippocampal cultures prepared from Het embryos. In these neurons, a 50% reduction of SNAP-25 levels was detected by quantitative immunocytochemistry in the somato-dendritic region and around 30% at axonal varicosities (Supplementary Figure S2A and B). Immunocytochemical staining for the synaptic vesicle protein SV2A, for the active zone component Bassoon, and for the postsynaptic scaffold protein PSD-95 was performed at 14 and 21 days *in vitro* (DIV) and percentages of colocalization among these proteins were quantified. Since the levels of SV2A do not differ between wt and Het cultures,²⁰ we used this protein as a reference marker. The percentage of juxtaposed pre- and postsynaptic terminals relative to the total presynaptic sites (SV2A&PSD-95/SV2A), the percentage of synapses showing immunoreactivity for the all three markers (SV2A&PSD-95&Bsn/SV2A) and the percentage of mature presynaptic terminals (SV2A&Bsn/SV2A) were quantified (Figures 2a–c). The increase in the first two parameters occurring in wt cultures between 14 and 21 DIV (Figure 2b) is consistent with the physiological maturation of synaptic contacts, while the lack of increase in the percentage of SV2A&Bsn/SV2A colocalizing puncta is in line with the earlier maturation of presynaptic relative to postsynaptic terminals, which is completed already at 14DIV.²⁸ A similar analysis, carried out in Het cultures, revealed a lack of postsynaptic maturation between 14 and 21DIV (Figure 2c).

To exclude the possibility that the alteration in PSD-95 density might result from a progressive decline of neuronal viability in culture, cell mortality was assessed by propidium iodide (PI) and calcein staining. While calcein emits green fluorescence signal in viable cells, PI reaches nuclei of dead cells only. Quantification of PI-positive/calcein-negative cells relative to the overall nuclei (labeled with Hoechst) indicated no difference in the extent of cell death between wt and Het cultures, at both 14DIV and 21DIV (Supplementary Figure S2C and D).

Consistently the fine morphological analysis of dendritic spines, performed in wt and Het GFP-transfected neurons at 21DIV, revealed a significant reduction in the number of mushroom spines and a parallel increase in the density of thin, filopodia-like protrusions (Figures 2d and e). A significant reduction in the number of PSD-95 puncta per unit length (Figures 2f and g) and a smaller PSD-95 cluster size (Figures 2f and h) were also detected in Het cultures relative to wt. Finally, miniature excitatory postsynaptic current (mEPSC) analysis in SNAP-25 Het networks revealed a significant reduction in both the frequency and the amplitude relative to controls (Figure 2i). Notably, no difference in mEPSC frequency and amplitude occurs in primary hippocampal cultures at earlier

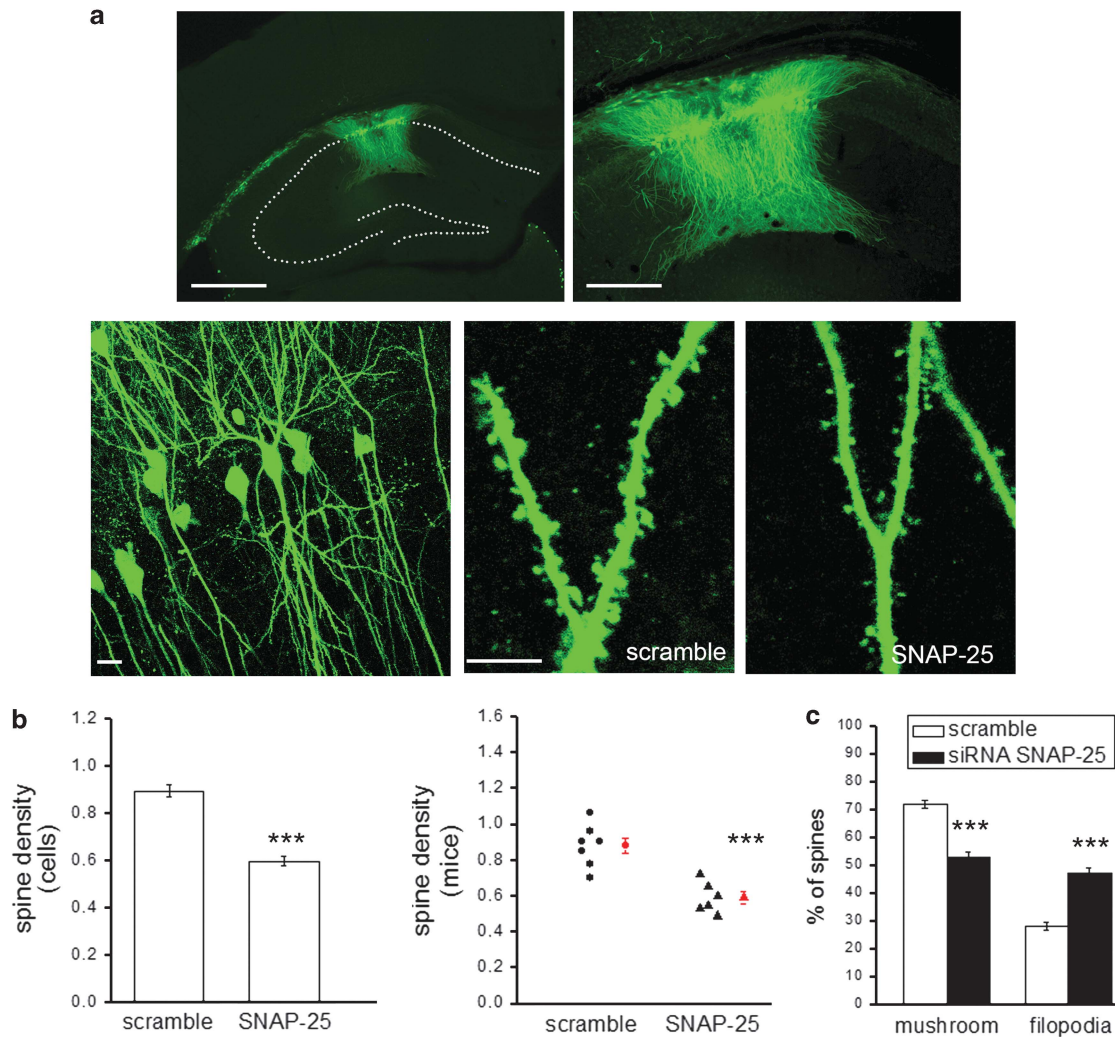


Figure 1 Altered spine morphology and density upon *in vivo* downregulation of SNAP-25. (a) Representative images of coronal slices showing an hippocampus injected with the lentiviral vector in the CA1 area (at different degrees of magnifications) and the secondary branches of apical dendrites of scramble and SNAP-25-shRNA treated mice (high magnification). Scale bars 400, 200, 20, and 10 μm , respectively. The white dotted line defines hippocampal structure. (b) Quantification of spine density in the CA1 field of scramble and SNAP-25-shRNA treated mice shows significant reduction of spine densities upon SNAP-25 downregulation (*left*, number of spines per μm (considering cells): scramble = 0.89 ± 0.03 ; SNAP-25-shRNA = 0.60 ± 0.02 ; Student's *t*-test, $P \leq 0.001$; *right*, number of spines per μm (considering animals) scramble: 0.88 ± 0.04 , $n = 7$; shSNAP-25: 0.59 ± 0.04 , $n = 6$; Student's *t*-test, $P < 0.001$). (c) Quantitative analysis of mushroom-type and thin filopodia-like spines percentage. Of note, SNAP-25-shRNA neurons show a decrease in mature spine number (mushroom-type), which is accompanied by an increase in thin spine number (filopodia-like) (percentage of spines: mushroom: scramble = 71.9 ± 1.4 ; SNAP-25-shRNA = 53 ± 1.7 ; Student's *t*-test, $P \leq 0.001$. Filopodia: scramble = 28.1 ± 1.4 ; SNAP-25-shRNA = 47 ± 1.7 ; Student's *t*-test, $P \leq 0.001$). Number of examined cells: scramble = 38, SNAP-25-shRNA = 36. Seven scramble and six SNAP-25-shRNA treated animals were analyzed and all data are expressed as mean \pm S.E.M. *** $P < 0.001$

developmental stages,^{18,20} thus confirming that morphological and functional postsynaptic defects become evident only at later stages during neuronal development.

A postsynaptic defect is responsible for the lack of plasticity occurring in networks constitutively developing in the presence of reduced SNAP-25 levels. Since SNAP-25 has crucial roles in the presynapse, the possibility exists that the postsynaptic defects might have resulted from a functional alteration at the presynaptic level, in turn leading to altered postsynaptic development. To address this possibility, we prepared mixed cultures of wt hippocampal neurons, from genetically modified mice constitutively expressing GFP under the beta-actin promoter,²⁹ and neurons

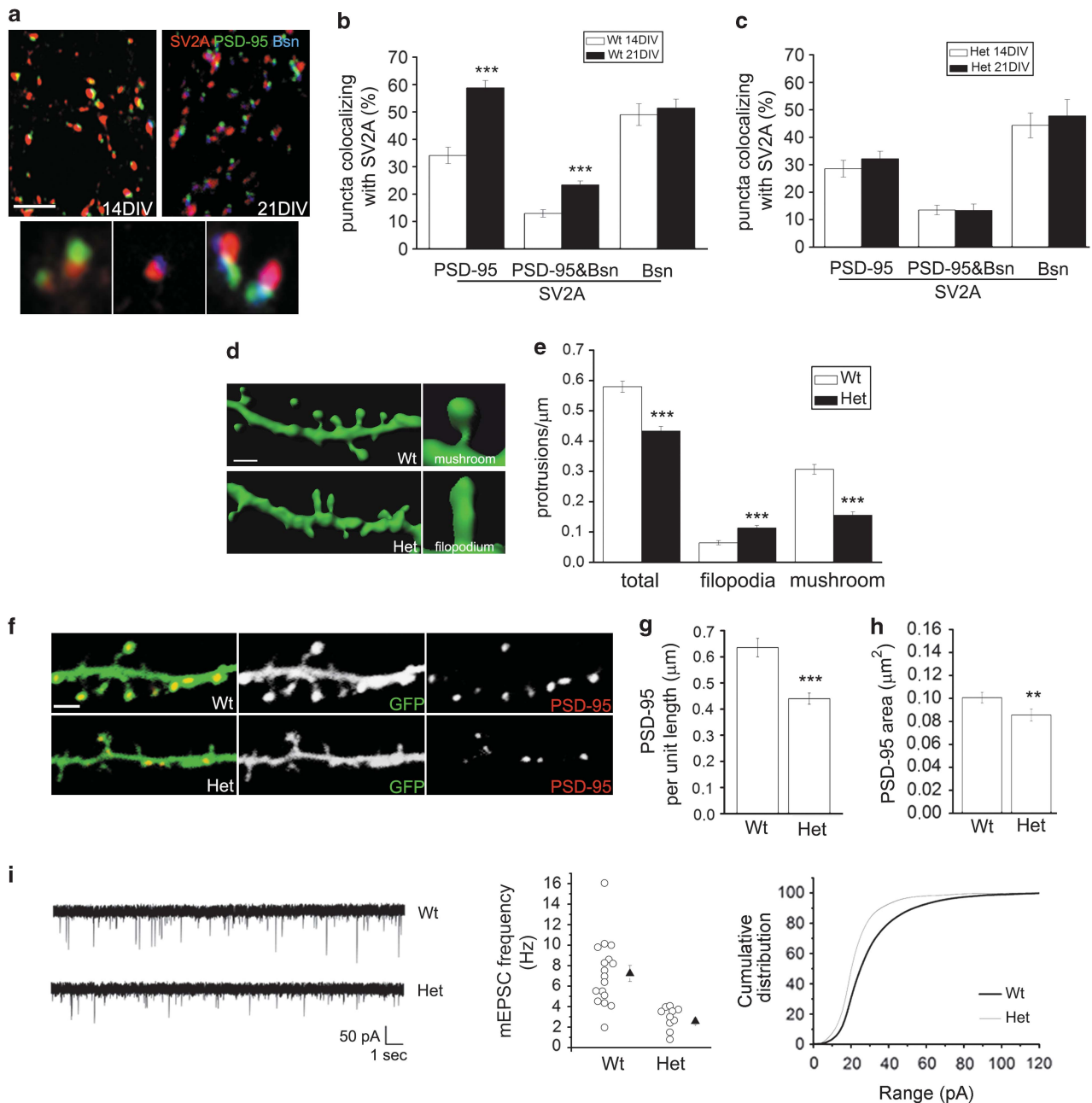
heterozygous for SNAP-25, originating from the same strain of mice, but not expressing GFP. Cultures were then maintained for 3 weeks before functional and morphological analysis. We generated two complementary experimental conditions. By plating wt-GFP and SNAP-25 Het neurons in a 1 : 10 ratio (wt-GFP/Het), the formation of networks in which several Het neurons impinged on a postsynaptic wt-GFP cell (Figure 3a) was favored. Conversely, plating SNAP-25 Het and wt-GFP neurons at an opposite ratio (Het/wt-GFP) favored the formation of networks in which Het neurons received most synaptic inputs from wt-GFP cells (Figure 3a'). Given the large excess of presynaptic inputs from Het neurons in the former setting, it would be reasonable to conclude that postsynaptic alterations in the wt-GFP neurons

would be the result of defective presynaptic function of SNAP-25 Het neurons. In contrast, in the latter setting, given the large excess of presynaptic inputs from wt neurons, it would be reasonable to conclude that a postsynaptic defect in SNAP-25 Het neurons results from a cell-autonomous, postsynaptic failure.

Interestingly, no difference in PSD-95 density was detected in wt-GFP neurons surrounded by Het neurons (Figure 3b), whereas RFP transfected SNAP-25 Het neurons receiving synaptic inputs from wt-GFP neurons (Het-RFP/wt-GFP) showed a significant reduction of PSD-95 puncta density relative to RFP-transfected wt neurons receiving from wt-GFP cells (wt-RFP/wt-GFP) (Figure 3b'). Consistently, electro-

physiological analysis showed that mEPSC frequency (Figure 3c) and amplitude (Figure 3d) of wt-GFP neurons grown together with a majority of Het neurons (wt-GFP/Het) did not differ with respect to control cultures of wt neurons. However, mEPSC frequency and amplitude of Het neurons cultured together with a majority of wt-GFP neurons (Het/wt-GFP) were significantly reduced with respect to control cultures. These data fully recapitulate the postsynaptic functional defects of SNAP-25 heterozygous cultures and rule out the possibility that functional defects in spines are secondary to presynaptic alterations.

It has been recently reported that the process of synaptic plasticity, that is, the ability of neurons to modify synaptic



function depending on external stimuli, is defective in neurons where the expression of SNAP-25 is acutely downregulated, both *in vitro* and *in vivo*.²² In particular, Jurado *et al.*²² have found that acute downregulation of SNAP-25 by lentiviral injection of acute hippocampal slices strongly impaired the generation of LTP in the CA1 region. We then asked whether neuronal networks constitutively developing in the presence of reduced SNAP-25, as occurring in psychiatric diseases, are able to compensate for this defect or display defective plasticity as well and, in the latter case, whether this could be univocally ascribed to a postsynaptic failure. Neuronal cultures were subjected to a chemical LTP protocol³⁰ consisting of an application of high doses of glycine for 3 min, which was followed by washout and immunolabeling for PSD-95, v-Glut1, and β III-tubulin after a 1-h recovery period. It has been shown that this procedure results in significant increase in the size of PSD-95-positive puncta and in a higher extent of colocalization of PSD-95 and v-Glut1 staining, in line with a potentiation of synaptic connections.³¹ Notably, in neurons heterozygous for SNAP-25, this protocol did not induce increases in either the size of PSD-95-positive puncta or the colocalization of pre and postsynaptic markers, whereas unmistakable increases were observed in wt neurons (Figures 3e and f).

The lack of potentiation in SNAP-25 Het cultures was also confirmed by electrophysiological recordings of mEPSCs. Indeed, while both the frequency (Figures 3g and h) and amplitude (Figures 3g and i) of mEPSCs significantly increased 35 min after glycine application in SNAP-25 wt neurons, no potentiation occurred in SNAP-25 Het neurons (Figures 3g–i).

To univocally ascribe the lack of potentiation to postsynaptic defects, we tested the ability of wt-GFP neurons cultured together with Het neurons (wt-GFP/Het) or Het neurons cultured together with wt-GFP neurons (Het/wt-GFP) (Figures 3j and k) to undergo synaptic potentiation. These experiments indicated that wt-GFP neurons receiving synaptic inputs from SNAP-25 Het neurons, when subjected to a

chemical LTP protocol, displayed potentiation levels that were similar to their control counterparts. By contrast, SNAP-25 Het neurons receiving synapses from wt neurons did not exhibit such potentiation (Figures 3j and k). These results indicate that genetic, moderate reductions of SNAP-25 levels impair synaptic plasticity and that a cell autonomous, postsynaptic defect is responsible for this defect.

PSD-95-dependent spine formation requires postsynaptic SNAP-25. PSD-95 is a major organizer of the postsynaptic density, playing a crucial role in determining spine size and morphology (El-Husseini *et al.*³²; reviewed in Sala *et al.*³³). Our data so far suggest that SNAP-25 reductions affect the localization and/or stabilization of PSD-95 in dendritic protrusions, influencing synapse organization and strength during development and plasticity. Consistent with this possibility, acute downregulation of SNAP-25 expression by siRNA,¹⁰ a treatment that reduces the protein expression by about 60%³⁴ (Supplementary Figure S2E) resulted in a significant reduction of PSD-95 area (Figures 4a and b). Notably, also the NR1 density and size was reduced upon acute reduction of SNAP-25, further confirming a postsynaptic defect (Supplementary Figure S4). The density (not shown, see also Tomasoni *et al.*²³) and the size (Figures 4a and b) of PSD-95 puncta were fully rescued by the overexpression, in the same neurons, of a mouse SNAP-25-GFP which is insensitive to the rat siRNA.

Overexpression of PSD-95, a procedure that results in the marked increase in spine volume and the enlargement of the postsynaptic densities (Nikonenko *et al.*³⁵; Figure 4c compare the first and the third bars), induced the formation of significantly smaller PSD-95-positive puncta in SNAP-25 siRNA-treated neurons relative to scramble-transfected neurons (Figures 4c and d). Therefore, postsynaptic SNAP-25 is required for proper PSD-95 accumulation and spine morphogenesis.

To investigate whether SNAP-25 controls the latter processes *via* its SNARE function, neurons were transfected with

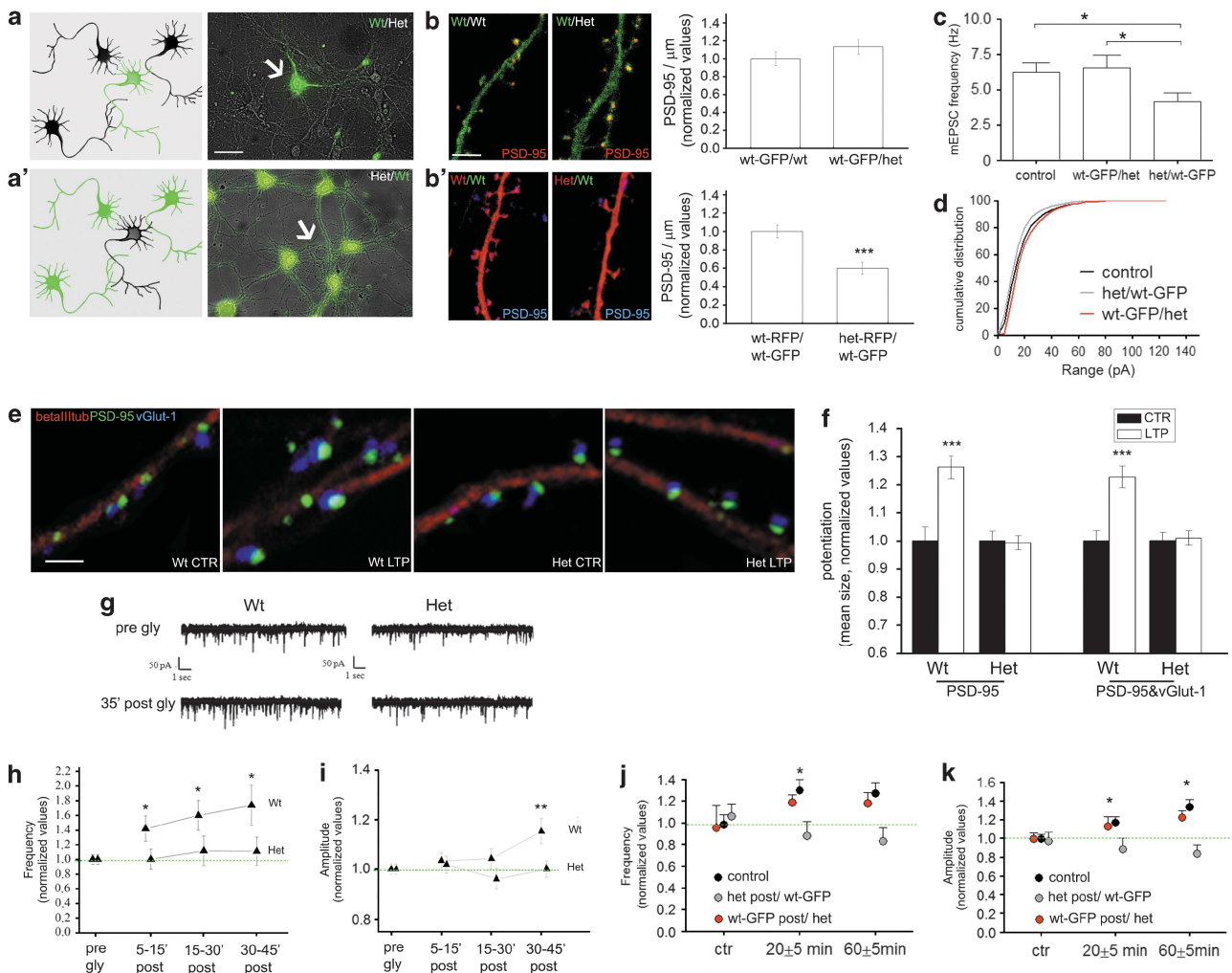
Figure 2 Structural and functional alterations in SNAP-25 heterozygous cultures. **(a)** Representative images of 14DIV and 21DIV wt cultures stained for the presynaptic markers SV2A (red), Bassoon (blue), and the postsynaptic protein PSD-95 (green). Scale bar: 5 μ m. **(b and c)** Quantification of the percentage of colocalizing puncta of juxtaposed pre- and postsynaptic terminals relative to the total presynaptic sites (SV2A&PSD-95/SV2A), the percentage of synapses showing immunoreactivity for the all three markers (SV2A&PSD-95&Bsn/SV2A) and the percentage of mature presynaptic terminals (SV2A&Bsn/SV2A) during development, in wt **(b)** and Het **(c)** cultures at 14 and 21 DIV. Postsynaptic maturation occurs in wt cultures between 14 DIV and 21DIV (wt 14DIV = SV2A&PSD-95/SV2A: 34.1 \pm 3.0; SV2A&PSD-95&Bsn/SV2A: 12.9 \pm 1.4; SV2A&Bsn/SV2A: 49 \pm 4.0, number of fields analyzed: 31; 21DIV = SV2A&PSD-95/SV2A: 58.8 \pm 2.7; SV2A&PSD-95&Bsn/SV2A: 23.4 \pm 1.5; SV2A&Bsn/SV2A: 51.4 \pm 3.2; number of fields analyzed: 27; Mann–Whitney rank-sum test $P \leq 0.001$; 3 independent experiments). A lack of postsynaptic maturation occurs in Het cultures during development (Het 14DIV = SV2A&PSD-95/SV2A: 28.5 \pm 3.0; SV2A&PSD-95&Bsn/SV2A: 13.5 \pm 1.8; SV2A&Bsn/SV2A: 44.3 \pm 4.5, number of fields analyzed: 20; 21DIV = SV2A&PSD-95/SV2A: 32.2 \pm 2.7, SV2A&PSD-95&Bsn/SV2A: 13.3 \pm 2.3; SV2A&Bsn/SV2A: 47.7 \pm 6.0, number of fields analyzed: 15; Mann–Whitney rank sum test $P = 0.397$, $P = 0.881$, and $P = 0.726$, respectively; 3 independent experiments). **(d)** Left, 3D reconstruction of dendritic shaft of neurons from 21DIV wt or Het cultures transfected with GFP; right, exemplary mushroom-type or filopodia-like spine. Scale bar 2 μ m. **(e)** Quantification shows a reduction in the number of total protrusions in Het neurons with respect to wt (number of protrusions per micron, wt = 0.58 \pm 0.02, number of examined dendrites: 83, number of neurons: 37; Het = 0.43 \pm 0.02, number of examined dendrites: 87; number of neurons: 45; Mann–Whitney rank-sum test $P \leq 0.001$; 3 independent experiments). The decrease in mature spine number (mushroom-type) is accompanied by an increase in thin spine number (filopodia-like) (number of mushroom spines per micron, wt: 0.31 \pm 0.02, number of examined dendrites: 63; number of neurons: 37; Het: 0.16 \pm 0.01, number of examined dendrites: 84; number of neurons: 45; number of filopodia-like spines per micron, wt: 0.06 \pm 0.01; Het: 0.11 \pm 0.01; Mann–Whitney rank-sum test $P \leq 0.001$; 3 independent experiments). **(f)** Representative images of 21 DIV wt and Het cultures transfected with GFP and immunostained for PSD-95 (red). **(g)** Quantification of PSD-95-positive puncta per unit length of parent dendrite (μ m) (wt = 0.64 \pm 0.04, number of examined dendrites: 88, number of neurons: 34; Het = 0.44 \pm 0.02, number of examined dendrites: 68, number of neurons: 33; Mann–Whitney rank-sum test $P < 0.001$; 3 independent experiments). **(h)** Quantification of PSD-95 puncta size reveals a significant reduction in Het neurons (in μ m², wt = 0.101 \pm 0.004, number of puncta: 433; number of analyzed neurons: 10; Het = 0.086 \pm 0.005, number of puncta: 354, number of analyzed neurons: 7; Mann–Whitney rank-sum test $P = 0.003$; 3 independent experiments). Data are expressed as mean \pm S.E.M. Scale bar 2 μ m. **(i)** Representative traces of mEPSCs from 21DIV wt or Het neurons followed by the corresponding quantitative analysis of miniature frequency (frequency (Hz) wt = 7.23 \pm 0.78; Het = 2.56 \pm 0.32; Student's *t*-test, $P \leq 0.001$) and amplitude (Amplitude (pA) wt = 37.67 \pm 2.3; Het = 29.61 \pm 0.99, cumulative probability; Kolmogorov–Smirnov test, $P < 0.05$; number of neurons: wt = 17, Het = 10; 2 independent experiments). ** $P < 0.01$; *** $P < 0.001$

a cDNA codifying for the BonT/E light chain, which cleaves SNAP-25 at its N-terminal side and prevents the protein entering the fusion complex.³⁶ Supplementary Figure 3 shows that cleavage of SNAP-25, assessed by the specific staining for the BonT/E-cleaved SNAP-25 fragment, does not significantly reduce spine density or PSD-95 size (Supplementary Figure 2B and C, see also Tomasoni *et al.*²³).

Since PSD-95 continuously migrates between synaptic and extra synaptic pools,^{37,38} we then reasoned that SNAP-25 could operate at the spine by restricting, either directly or indirectly, PSD-95 mobility. We therefore measured the dynamics of synaptic PSD-95 upon acute reduction of SNAP-25 expression by siRNA, using fluorescence recovery after photobleaching (FRAP) analysis. To carry out PSD-95 FRAP analysis, we selected spines with similar morphologies in siRNA- or scramble-treated cultures, 4–5 days after transfection. PSD-95-GFP bleaching, followed by temporal analysis of fluorescence recovery over the next 40 s (Figure 4d), revealed a significantly larger mobile fraction of PSD-95 in acutely SNAP25-downregulated cells compared with scramble control cells (Figure 4e). These data indicate that SNAP-25 affects PSD-95 localization and mobility through a mechanism, which does not involve its fusion

activity, but rather implicates a scaffolding, protein–protein interaction role.

SNAP-25 is part of the postsynaptic protein complex containing PSD-95. To assess whether SNAP-25 controls PSD-95 mobility through direct participation to the PSD complex, we performed Proximity Ligation Assay (PLA) in cultured neurons to evaluate an *in situ* complex formation. The results revealed a significantly higher signal for SNAP-25 and PSD-95 compared with PSD-95 and the merely presynaptic protein Piccolo (Figures 5a and b), suggesting that PSD-95 and SNAP-25 can be part of the same complex in their natural cellular environment. To further probe the possible existence of a postsynaptic protein network including SNAP-25, we applied a Luminescence-based Mammalian intERactome (LUMIER) assay^{39,40} to test the following protein–protein interactions: SNAP-25 and PSD-95; PSD-95 and p140Cap (SRCIN1). The rationale for including p140Cap in the assay results from our previous demonstration that acute downregulation of SNAP-25 impairs spines morphogenesis through p140Cap,²³ a synaptic protein involved in Src-kinase regulation and microtubules organization inside the spine.⁴¹ The well-characterized protein/protein interaction



Bcl2-BAD⁴² served as a positive control. The bait protein fused to a protein-A tag and linked to a Renilla Luciferase and the prey protein fused to a Firefly Luciferase were co-expressed in HEK293 cells for 48 h. After cell lysis, protein complex formation was assessed by Firefly Luciferase activity of the co-immunoprecipitated prey fusion protein (Figure 5c). Results indicated that SNAP-25 and PSD-95 do not interact directly, whereas p140Cap specifically interacts with PSD-95 (Figure 5c). Given that p140Cap interacts with SNAP-25,⁴¹ an indirect association of SNAP-25 and PSD-95 potentially mediated by p140Cap may occur at the post-synaptic level. To test this hypothesis, we performed immunoprecipitation of PSD-95 from wt and p140Cap null brain lysates. Figure 5d shows that in wt brain the spine protein p140Cap^{23,41} and SNAP-25 co-immunoprecipitated with PSD-95, whereas in p140Cap null brain a significantly less amount of SNAP-25 co-immunoprecipitated with PSD-95, suggesting the existence, in the spine, of a novel postsynaptic network of proteins formed by SNAP-25, p140Cap, and PSD-95.

Discussion

Variations in dendritic spine number and morphology occur both during development and in adulthood, allowing the establishment and remodeling of neuronal circuits. Spine structural plasticity is tightly coordinated with synaptic function, with spine enlargement occurring during long-term potentiation and spine shrinkage during long-term depression.⁴³ In the present study, we demonstrate an unexpected defect in dendritic spine morphology in SNAP-25 Het neurons after 3 weeks in culture. At this time,

SNAP-25 Het neurons display a lower density of spines, which appear longer than controls. Consistently, SNAP-25 Het cultures display a reduction in both frequency and amplitude of mEPSCs and are unable to undergo a common form of experimentally induced potentiation. Moreover, rats injected with viral vector harboring shRNA to SNAP-25 into the gustatory cortex display an impaired taste memory similarly to rats injected with viral vector expressing shRNA to PSD-95.⁴⁴

During development, synapse formation is directed by reciprocal signaling between pre- and postsynaptic neurons. Synaptic organizing proteins stabilize early synaptic contacts *via* recruitment of synaptic vesicles to the presynaptic active zone and NMDA receptors to the postsynaptic density. PSD-95 thereby acts as a major organizer of signaling complexes at the postsynaptic membranes and serves as scaffold for the recruitment of synaptic components required for synapse development. PSD-95 appears very early at nascent synapses³⁷ where it clusters NMDA receptors^{45,46} and controls synaptic AMPA receptors number, thus determining synaptic strength.^{47,48} Our data indicate that PSD-95 has the ability to bind p140Cap, thus forming a complex with SNAP-25, and that acute downregulation of SNAP-25 leads to PSD95 destabilization, probably affecting the stability of the postsynapse and impairing synaptic plasticity.

Although different models concerning the dynamic aspects of synaptogenesis have been proposed, presynaptic differentiation appears to occur slightly faster than postsynaptic development.^{49,50} Cycling of synaptic vesicle protein transport vesicles at predefined sites along the axon appears to selectively attract dendritic filopodia and initiate synapse formation.⁵¹ Furthermore, although vesicular glutamate

Figure 3 A postsynaptic defect impairs plasticity in SNAP-25 heterozygous cultures. **(a and a')** Schematic representation and representative images of the two experimental settings used for mixed wt-GFP/Het neurons. Scale bar: 20 μ m. See also Antonucci *et al.*²⁰ and **(e)**. **(b and b')** Left, representative images of wt-GFP/Het mixed cultures transfected with GFP or RFP as indicated and stained for PSD-95. Right, analysis of density of PSD-95 puncta in wt-GFP/Het mixed cultures. Results show no difference in PSD-95 density in wt neurons surrounded by either Het or wt neurons **(b)**, PSD-95 puncta per unit length: wt-GFP/wt = 1.00 ± 0.08 , number of examined dendrites: 45, number of neurons: 16; wt-GFP/Het = 1.13 ± 0.08 , number of examined dendrites: 63, number of neurons: 27; Mann-Whitney rank-sum test $P = 0.481$ whereas a significant decrease in the density of PSD-95 puncta is observed in Het neurons surrounded by either wt or Het neurons **(b')**, PSD-95 puncta per unit length: wt-RFP/wt-GFP = 1.00 ± 0.07 , number of examined dendrites: 9, number of neurons $n = 4$; Het-RFP/wt-GFP = 0.6 ± 0.07 , number of examined dendrites: 21, number of neurons: 8; normalized values; Mann-Whitney rank-sum test $P \leq 0.001$). Data are expressed as mean \pm S.E.M. (normalized values). Scale bar: 2 μ m. **(c)** mEPSC recordings of wt-GFP surrounded by Het neurons or of Het neurons surrounded by wt-GFP neurons reveal a significant reduction in mEPSC frequency in the latter condition. **(d)** A reduction of mEPSC amplitude is also evident (frequency (Hz) control = 6.22 ± 0.67 , number of cells: 13; wt-GFP/Het = 6.53 ± 0.92 , number of cells: 10; Het/wt-GFP = 4.14 ± 0.64 , number of cells: 9; control *versus* Het/wt-GFP $P = 0.02$, wt-GFP/Het *versus* Het/wt-GFP $P = 0.03$, Mann-Whitney rank-sum test; amplitude (pA), control = 19.78 ± 1.01 ; wt-GFP/Het = 19.04 ± 1.6 ; Het/wt-GFP = 17.01 ± 1.08 ; control *versus* Het/wt-GFP $P = 0.005$; wt-GFP/Het *versus* Het/wt-GFP $P = 0.005$; Kolmogorov-Smirnov test; 3 independent experiments). **(e)** Representative images of wt and Het cultures before and after performing a chemical LTP procedure. Cultures were stained for β III tubulin (red), PSD-95 (green), and v-Glut1 (blue). Scale bar depicts 2 μ m. **(f)** Extent of potentiation is represented by the quantification of the mean size of PSD-95-positive clusters and by the PSD-95&vGlut1 colocalization area. Potentiation occurs in wt but not in Het cultures (PSD-95 size: wt ctr: 1.00 ± 0.05 , wt LTP: 1.26 ± 0.04 , Het ctr: 1.00 ± 0.03 , Het LTP: 0.99 ± 0.03 . PSD-95&v-Glut1 size: wt ctr: 1.00 ± 0.03 , wt LTP: 1.23 ± 0.04 , Het ctr: 1.00 ± 0.03 , Het LTP: 1.01 ± 0.03 . Number of analyzed fields: wt ctr: 46, wt LTP: 50, Het ctr: 62, Het LTP: 75. Mann-Whitney rank-sum test, $P \leq 0.001$; 3 independent experiments). Data are expressed as mean \pm S.E.M.; normalized values. **(g-i)** Electrophysiological recordings of mEPSCs before and after chemical LTP induction in wt and Het neurons (5 min before LTP application, 15, 30, and 45 min after LTP application). **(g)** Representative mEPSC traces. Differently from wt, Het neurons are unable to undergo LTP. **(h)** mEPSC frequency (normalized values): wt pre gly: 1 ± 0.06 ($n = 29$), wt post 5': 1.4 ± 0.17 ($n = 20$); wt post 30': 1.59 ± 0.20 ($n = 17$); wt post 45': 1.73 ± 0.27 ($n = 10$); Het pre gly: 1 ± 0.06 ($n = 15$); Het post 5': 1.00 ± 0.13 ($n = 14$); Het post 30': 1.11 ± 0.20 ($n = 10$); Het post 45': 1.10 ± 0.19 ($n = 10$). wt pre gly *versus* wt post 5': $P < 0.021$, wt pre gly *versus* wt post 30': $P < 0.012$, wt pre gly μ m wt post 45': $P < 0.014$. Mann-Whitney rank-sum test. **(i)** mEPSC amplitude (normalized values): wt pre gly: 1 ± 0.02 ; wt post 5': 1.03 ± 0.03 ; wt post 30': 1.04 ± 0.04 ; wt post 45': 1.15 ± 0.05 ; Het pre gly: 1 ± 0.02 ; Het post 5': 1.02 ± 0.03 ; Het post 30': 0.96 ± 0.04 ; Het post 45': 1 ± 0.03 . wt pre gly μ m wt post 45': $P = 0.001$. Student's *t*-test. n is the number of cells. Four independent experiments. **(j and k)** mEPSC frequency and amplitude recorded from neurons in mixed cultures experimental settings were normalized to values obtained before glycine application. Note that wt-GFP neurons surrounded by Het neurons undergo LTP, whereas Het neurons surrounded by wt-GFP neurons fail to potentiate (frequency (Hz) pre-gly: control = 0.99 ± 0.09 ($n = 16$), wt-GFP/Het = 0.96 ± 0.2 ($n = 5$), Het/wt-GFP = 1.06 ± 0.11 ($n = 8$); 20 \pm 5 min: control = 1.30 ± 0.1 ($n = 15$), wt-GFP/Het = 1.19 ± 0.07 ($n = 3$), Het/wt-GFP = 0.88 ± 0.13 ($n = 8$); 60 \pm 5 min: control = 1.27 ± 0.1 ($n = 7$), wt-GFP/Het = 1.18 ± 0.10 ($n = 2$), Het/wt-GFP = 0.83 ± 0.13 ($n = 5$); n is the number of cells; ctr *versus* ctr 20 min: $P = 0.04$, Mann-Whitney rank-sum test. Amplitude (pA) pre-gly: control = 0.99 ± 0.04 , wt-GFP/Het = 0.99 ± 0.07 , Het/wt-GFP = 0.97 ± 0.09 ; 20 \pm 5 min: control = 1.17 ± 0.06 , wt-GFP/Het = 1.13 ± 0.10 , Het/wt-GFP = 0.88 ± 0.12 ; 60 \pm 5 min: control = 1.34 ± 0.08 , wt-GFP/Het = 1.23 ± 0.07 , Het/wt-GFP = 0.84 ± 0.09 ; ctr *versus* ctr 20 min: $P = 0.03$, ctr *versus* ctr 60 min: $P = 0.2$; Mann-Whitney rank-sum test; 3 independent experiments). Data are expressed as mean \pm S.E.M. * $P < 0.05$; ** $P < 0.01$; *** $P < 0.001$

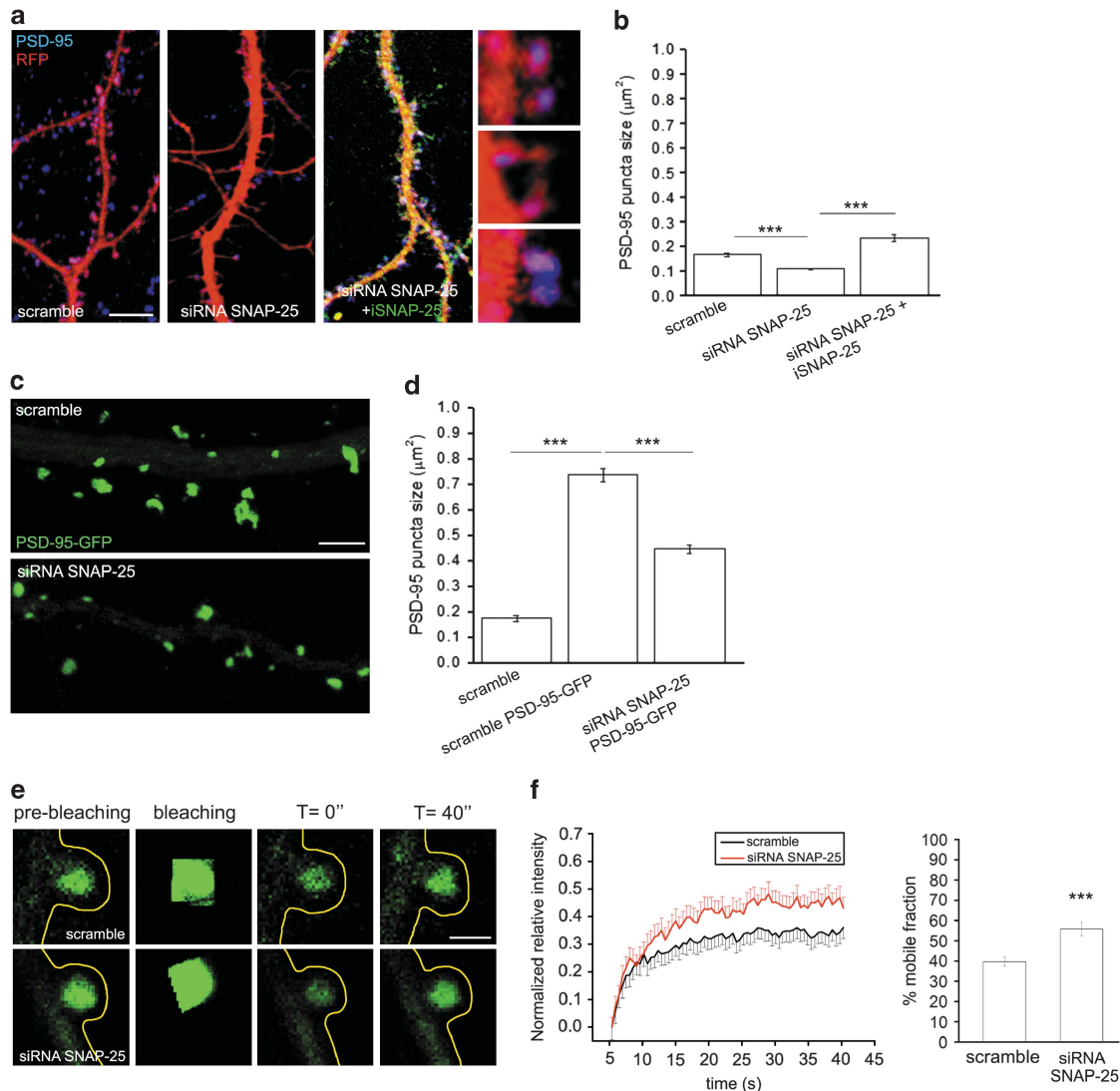


Figure 4 PSD-95-dependent spine formation requires postsynaptic SNAP-25. **(a)** Representative images of dendrite portions of neurons transfected with (left) RFP and a scramble construct, or (middle) RFP and a construct silencing SNAP-25 (siRNA), or (right) RFP and a rat construct silencing SNAP-25 plus a mouse siRNA-insensitive SNAP-25-GFP (iSNAP-25-GFP) construct. All neurons are stained for PSD-95 (blue). Right, high magnification images of scramble, siRNA or siRNA plus SNAP-25-GFP spines. Scale bar: $6\ \mu\text{m}$ for low mag images and $1.5\ \mu\text{m}$ for high mag images. **(b)** Quantification of the size of PSD-95 puncta (in μm^2 , scramble = 0.16 ± 0.01 , number of analyzed puncta: 305, number of analyzed neurons: 45; siRNA SNAP-25 = 0.11 ± 0.01 , number of analyzed puncta: 180, number of analyzed neurons: 40; SNAP-25-GFP+siRNA SNAP-25 = 0.23 ± 0.01 , number of analyzed puncta: 117, number of analyzed neurons: 18. Kruskal-Wallis one-way analysis of variance on ranks $P \leq 0.001$; 3 independent experiments for SNAP-25-GFP+siRNA SNAP-25 condition, 6 independent experiments for scramble and silencing conditions). Data are expressed as mean \pm S.E.M. **(c and d)** Representative images of proximal dendrite shafts cotransfected with PSD-95-GFP and a scramble or siRNA construct for SNAP-25, respectively, and the relative quantification of the size of PSD-95 puncta (in μm^2 , scramble = 0.17 ± 0.01 , number of analyzed puncta: 152, number of analyzed neurons: 21; scramble PSD-95-GFP = 0.74 ± 0.02 , number of analyzed puncta: 203, number of analyzed neurons: 24; siRNA SNAP-25 PSD-95-GFP = 0.45 ± 0.02 , number of analyzed puncta: 296, number of analyzed neurons: 28. Mann-Whitney rank-sum test $P \leq 0.001$; 3 independent experiments). Data are expressed as mean \pm S.E.M. Scale bar: $2\ \mu\text{m}$. **(e and f)** FRAP measurements of PSD-95-GFP in spines of siRNA-treated or scramble-treated neurons. **(e)** Representative images of the same area before photobleaching (Pre-bleaching), at $t=0$ and 40 s after photobleaching of scramble- and siRNA-treated neurons. Neurons were maintained at $37\ ^\circ\text{C}$ during the experiment. Scale bar: $1\ \mu\text{m}$ for each image. **(f)** Left, FRAP curves of PSD-95-GFP in spines over a 40-s period. Number of analyzed spines: 58 for scramble-treated neurons; 52 for siRNA-SNAP-25-treated neurons. Right, histogram showing the increase in mobile fraction of PSD-95-GFP in siRNA-treated spines with respect to scramble-treated spines (scramble = 39.72 ± 2.09 ; siRNA-SNAP-25 = 55.81 ± 3.30 ; Mann-Whitney rank-sum test $P \leq 0.001$; 4 independent experiments). Data are normalized and expressed as mean \pm S.E.M. *** $P < 0.001$

release is not required for excitatory synapse formation,^{52,53} the number of synapses formed in the absence of neurotransmitter release is dramatically decreased,⁵⁴ suggesting that glutamate release could influence excitatory synaptogenesis.⁵⁵ Given that SNAP-25 has a critical role at the presynaptic terminal during synaptic vesicle fusion and considering the possible role of presynaptic function in the

maturation of the postsynaptic compartment, the postsynaptic effects observed here might have been the result of SNAP-25-related alterations in presynaptic release,⁷ even if electron microscopy studies showed that reduced levels of SNAP-25 do not alter the presynaptic terminal structure and vesicles content.⁵⁶ By taking advantage of mixed cultures of wt and Het neurons, we demonstrated that postsynaptic defects in

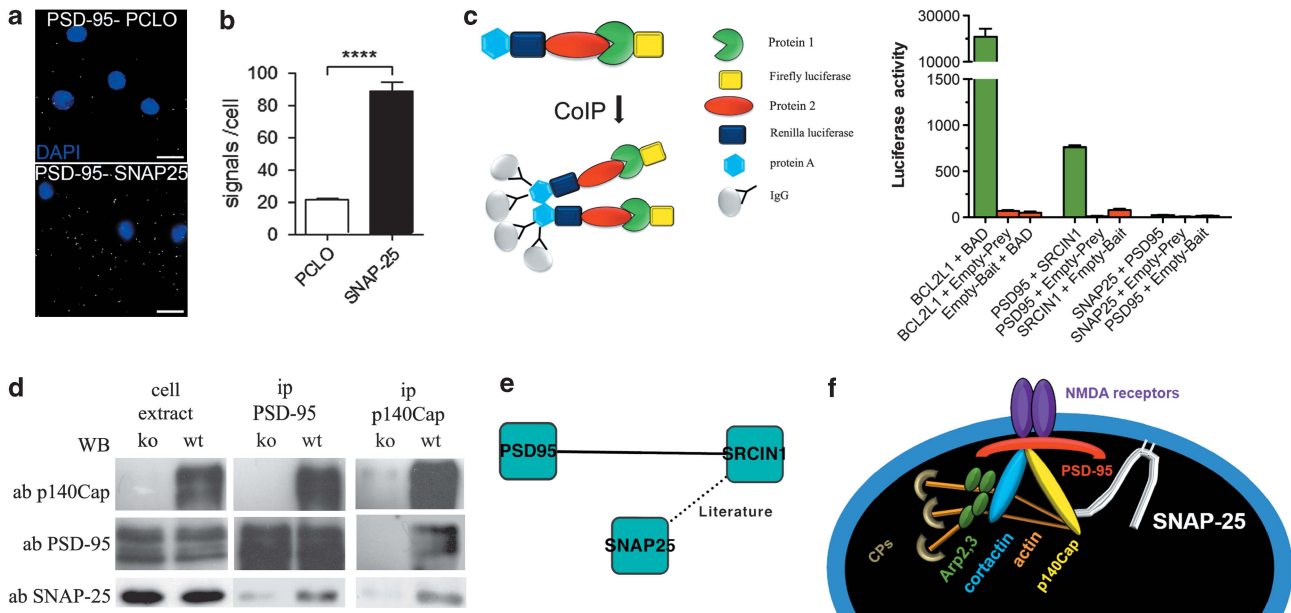


Figure 5 SNAP-25 and PSD-95 are part of the same molecular complex in the brain. (a) Representative images obtained from Proximity Ligation experiments. Neurons were incubated with primary antibodies against PSD-95/PCLO or PSD-95/SNAP-25 after which PLA probes were added, ligated, amplified and detected with a Cy3 probe. (b) Quantification of PLA signals per neuron. PLA signals: 21.1 ± 0.9 per nucleus in PSD-95/PCLO stained cells (34 analyzed cells); 88.3 ± 6.3 per nucleus in PSD-95/SNAP-25 stained cells (32 analyzed cells); $****P \leq 0.0001$, unpaired *t*-test. (c) Left, scheme representing the LUMIER co-immunoprecipitation assay. Right, interactions between the tested proteins in HEK293 cells as detected by LUMIER co-immunoprecipitation assay. The green bar indicates a specific interaction, evaluated in term of firefly luciferase activity. Red bars are controls. (d) Brain extracts were prepared as in Materials and Methods and immunoprecipitated as indicated, and run on SDS-PAGE. Western blot was performed with antibodies to p140Cap, PSD-95, and SNAP-25. (e) Summary of the proteins' interactions according to LUMIER assay results and literature. (f) Model of interaction in the postsynaptic compartment: SNAP-25 and PSD-95 interact through p140Cap

SNAP-25 Het neurons do not stem from alterations in the presynaptic terminal, but are instead related to a cell-autonomous impairment at the postsynaptic compartment.

In recent years SNARE/SM proteins have been shown to be involved in activity-dependent AMPA receptor exocytosis during LTP²² and SNAP-25, in particular, has been reported to have a role in the removal of kainate receptors from the postsynaptic membrane,⁵⁷ in the insertion of NMDA receptors in neuronal plasma membrane²¹ and of P/Q and L type-voltage gated calcium channels.^{10,58} Also, acute regulation of SNAP-25 expression has been found to impair synaptic plasticity probably affecting NMDAR trafficking.²² Our data indicate that SNAP-25 has also a structural role in the postsynaptic compartment by interacting with the postsynaptic protein p140Cap, which in turn binds to PSD-95. The integrity of this macromolecular complex appears to be fundamental for both structural and functional synaptic plasticity. Indeed, p140Cap^{-/-} mice display similar defects in episodic memory and are impaired in LTP and in LTD.⁵⁹ These data provide new mechanistic insights as to SNAP-25 involvement in synaptopathies that go beyond the protein's known roles in presynaptic function, indicating a protein role as a post-synaptic structural hub. Indeed, the activity-driven spine remodeling is defective in neuronal networks constitutively developing in the presence of reduced levels of SNAP-25, as it might presumably occur in human pathologies, such as schizophrenia, where both a reduction of SNAP-25 expression¹⁵ and a reduction in dendritic spine density⁶⁰ have been described.

Materials and methods

Animals. All the experimental procedures followed the guidelines established by the Italian Council on Animal Care and were approved by the Italian Government decree No. 27/2010. All efforts were made to minimize the number of subjects used and their suffering. SNAP-25 wild-type and SNAP-25 heterozygous male mice⁶¹ were housed in cages with free access to food and water at 22 °C and with a 12-h alternating light/dark cycle. Genotyping was performed by PCR as described in Washbourne *et al.*⁶¹ p140Cap wild-type and knockout mice strain is described in Repetto *et al.*⁵⁹

Cell cultures. Mouse hippocampal or rat hippocampal and cortical neurons were prepared from E18 fetal SNAP-25 heterozygous (Het) or wild-type (wt) littermates C57BL/6 mice as described in Bartlett and Banker⁶² with slight modifications. Briefly, hippocampi were dissociated by treatment with trypsin (0.125% for 15 min at 37 °C), followed by trituration with a polished Pasteur pipette. The dissociated cells were plated onto glass coverslips coated with poly-L-lysine at density of 400 cells/mm². The cells were maintained in Neurobasal (Invitrogen, San Diego, CA, USA) with B27 supplement and antibiotics, 2 mM glutamine, and 12.5 μM glutamate (neuronal medium).

Mixed cell cultures. Primary hippocampal GFP-positive neuronal cultures were prepared from the hippocampi of E18 fetal C57BL/6 GFP transgenic mice,²⁹ with the GFP gene controlled by the actin promoter. To isolate the neuronal type of interest among wild-type or SNAP-25 heterozygous neurons, GFP-positive neurons were co-cultured with SNAP-25 Het or wt neurons in a ratio of 1 to 10 or 10 to 1.

DNA constructs and expression. Neuronal cultures were transfected at 17DIV with pEGFP-C1 (Clontech, Palo Alto, CA, USA) or pSUPER-DsRed plasmid (obtained from pSUPER-GFP, Oligoengine, Seattle, WA, USA) and FU(PSD95:EGFP) W.⁶³ Silencing of SNAP-25 was achieved via transfection of a pSUPER construct.^{10,58} A non-specific siRNA duplex of the same nucleotides but in an irregular sequence (scrambled SNAP-25 siRNA) was prepared using oligonucleotides 5-GATCCCCG AGGAGTTATGCGATAGTATTCAAGAGAATGATACGCTATTGAGGAGTTTTTGGAAA-3 and 5-AGCTTTTCCAAAAAACCCTCAATACGCTATCTCTTGAATACTATCGCATA

ACTCTCGGG-3 that were annealed and ligated into the pSuper vector as described previously.^{10,58}

For LUMIER assay, mouse *Srcin1* was PCR amplified using Phusion Hot Start II High-Fidelity DNA Polymerase (Thermo Scientific, Waltham, MA, USA) and the following primers: 5-GGGGA;CAAGTTGTACAAAAAGCAGGCTTCATGGGGA ACGCTCCGTCCCAAG-3 and 5-GGACCACTTTGTACAAGAAAGCTGGGTCGG AAGGAGATGGAAGAATTCCTTGC-3. The PCR product was inserted into pDONR221 using the BP clonase (Invitrogen), amplified and further shuttled into the LUMIER prey vector (FireV5DM). Human full-length cDNA clones of SNAP25, PSD95, and CTTN were available as entry clones and shuttled into the respective LUMIER bait (PAReniDM) and prey (FireV5DM) vectors.

Lentiviral constructs. A short hairpin RNA construct directed against SNAP-25 was generated by PCR and subcloned into a lentiviral vector plasmid (pLKO.1-puro-CMV-tGFP, Sigma-Aldrich, Rehovot, Israel). A scrambled shRNA sequence was generated in a similar way and served as a control. The SNAP-25 or scrambled U6-shRNA expression cassettes were co-expressed with eGFP driven by CMV promoter. High titer lentiviral vectors were produced by a transient transfection of the third-generation transfer, packaging and envelope plasmid set into 293FT cell line (Invitrogen, Carlsbad, CA, USA), and allowed to express and form viral particles for 48 h. Then the medium was collected; the viral particles were purified and concentrated by multiple centrifugation steps, dissolved in sterile PBS, aliquot and stored at -80°C until further use. Viral titer was determined using the FACS analysis. A titer higher than 10^8 tu/ml was used for the experiments.

Lentiviral injections. C57BL6N mice (Charles River Laboratories, Calco, Italy) were deeply anesthetized (100 mg/kg Ketamine (KETAVET, INTERVET), 10 mg/kg Xilazina (Rompun, BAYER) in physiologic solution) and placed on a stereotaxic frame (Kopf Instruments, Tujunga, CA, USA). The viral suspension was delivered *via* glass needle attached to a 10- μl Hamilton syringe. Bilateral injection (2 μl /each) was performed in the CA1 area of dorsal hippocampus (coordinates of injection: anteroposterior -2.0 , lateral ± 1.5 , dorsoventral -1.1 from duramide surface) at a rate of 1 $\mu\text{l}/\text{min}$. Coordinates of injection were calculated from the Bregma level according to Paxinos and Franklin Mouse Brain Atlas⁶⁴ under microscope guide (L-0940SD, INAMI). The needle remained in place for an additional 5 min to facilitate the controlled delivery of the virus. The titer of the SNAP-25-shRNA virus is 2.3×10^9 tu/ml and for the scramble 5×10^8 tu/ml. Stereotaxic injections into the gustatory cortex were performed as described.⁴⁴

Immunocytochemical staining. Neuronal cultures were fixed with 4% paraformaldehyde+4% sucrose, or with 100% cold methanol, depending on the markers. The following antibodies were used: rabbit anti-SV2A (1:1000; Synaptic Systems, Goettingen, Germany), guinea pig anti-Bassoon (1:300; Synaptic Systems), guinea pig anti-vGLUT1 (1:1000; Synaptic Systems), mouse anti-PSD95 (1:400; UC Davis/NIH NeuroMab Facility, CA), rabbit anti-GFP (1:400; Invitrogen, San Diego, CA, USA), mouse anti-beta III tubulin (1:400; Promega Corporation, Madison, WI, USA), rabbit anti-tubulin (1:80; Sigma-Aldrich, Milan, Italy), rabbit anti-MAP2 (Millipore, Billerica, MA, USA), mouse anti-SNAP-25 (1:1000; SMI81 Sternberger Monoclonals, Baltimore, MD, USA). Secondary antibodies were conjugated with Alexa-488, Alexa-555, or Alexa-633 fluorophores (Invitrogen). Images were acquired using a Leica SPE confocal microscope equipped with an ACS APO $\times 63/1.30$ oil objective (Leica Microsystems, Solms, Germany). Image analysis was performed using the ImageJ software (NIH, Bethesda, MD, USA). Dendritic spines were classified according the following parameters: mushroom (length $\leq 1.2 \mu\text{m}$, width $\geq 0.5 \mu\text{m}$); filopodia (length $> 1.2 \mu\text{m}$, width $< 0.5 \mu\text{m}$), in line with.⁶⁵ Colocalization of two or three selected markers was measured using the boolean function 'AND' for the selected channels. The resulting image was binarized and used as a colocalization mask to be subtracted to single channels. The number of the puncta resulting from colocalization mask subtraction was measured for each marker. A colocalization ratio was set as colocalizing puncta/total puncta number.

Immunohistochemical staining. Experiments were performed on C57BL/6 mice. Animals were anesthetized with chloral hydrate (4%; 1 ml/100 g body weight, i.p.) and perfused with 4% paraformaldehyde. The brain was postfixed and coronally cut with a Vibratome in 50- μm -thick serial sections. Immunofluorescence staining was carried out on free-floating sections as described in Frassoni *et al.*⁶⁶ Free-floating sections were processed for rabbit anti-GFP (1:400, Invitrogen) followed by incubation with secondary antibody Alexa-488 fluorophore (Invitrogen) and mounted

in Fluorsave (Calbiochem, San Diego, CA, USA). Sections were examined by means of a Zeiss LSM 510 META confocal microscope (Leica Microsystems). The images were acquired using a $\times 40$ oil immersion lens (numerical aperture 1.0) with additional electronic zoom factor up to 4. Up to 10 different neurons were acquired and analyzed for each animal.

Co-immunoprecipitation. Brain tissues were frozen in liquid nitrogen. Proteins were extracted from mice brain with lysis buffer (1% Triton X-100, 150 mM sodium chloride, 50 mM Tris-HCl pH 7.5, protease inhibitors (Roche, Basel, Switzerland), 1 mM phenylmethylsulfonyl fluoride, 1 mM sodium vanadate, 1 mM sodium fluoride, 1 mM DTT). For immunoprecipitation (IP) assays, 5 mg of total extract was immunoprecipitated for 2 h at 4°C with specific or unrelated antibodies in the presence of Dynabeads Protein G (Invitrogen). The proteins were resolved by reducing SDS-polyacrylamide gel electrophoresis and transferred onto nitrocellulose filters, which were incubated with the indicated antibodies and developed with ECL system. The following antibodies were used: PSD-95 (1:4000, monoclonal; UC Davis/NIH NeuroMab Facility, CA); SNAP-25 (1:10 000, Synaptic System); mouse monoclonal to p140Cap for western blot was homemade produced as described in Di Stefano *et al.*⁶⁷

LUMIER assay. The Lumier assay was performed as described previously.⁴⁰ Briefly, PSD-95, *Srcin1*, and SNAP-25 were cloned into the bait PA-Renilla luciferase vector and/or into the prey firefly luciferase vector using the gateway technology (Invitrogen). Vectors were co-transfected into HEK293 cells using jetPEI transfection reagent (Polyplus, New York, NY, USA) and 48 h after transfection lysed in HEPES-lysis buffer (50 mM HEPES, 150 mM NaCl, 10% glycerol, 1% NP-40, 20 mM NaF, 1.5 mM MgCl_2 , 1 mM EDTA, 1 mM DTT, $1 \times$ Benzamide, $1 \times$ Protease Inhibitor Cocktail -EDTA (Roche, Basel, Switzerland), 1 mM PMSF). In all, 384-well high-binding white microplates (Greiner, Kremsmünster, Austria) were coated with sheep-gamma globulin (Dianova, Hamburg, Germany) and rabbit anti-sheep IgG (Dianova). Bait and prey protein expression was confirmed by measuring Renilla and Firefly luciferase activity of the crude lysates. Baits were immunoprecipitated from cell extracts *via* the PA-tag and immunoprecipitation and co-immunoprecipitation evaluated by renilla and firefly activity, respectively. Luciferase activities were determined using the Dual-Glo Luciferase Kit (Promega) in a luminescence plate reader (TECAN Infinite M1000). To determine background protein binding, bait protein binding to empty prey vectors, as well as prey protein binding to empty bait vector were determined as well.

Proximity ligation assay. Proximity ligation assay was performed according to the manufacturer's protocol using custom blocking solutions during antibody incubations (Olink Bioscience, Uppsala, Sweden). Briefly, rat cortical neurons were grown at low density (34 000 cells/ cm^2) on coverslips for 2DIV before AraC (5 μM , Sigma, Milan, Italy) was added to inhibit glial growth and enable signal quantification per neuronal cell. Cells were grown further till 14DIV and then fixed with 4% PFA, washed with PBS and permeabilized with 0.2% TX-100 in PBS for 2 min. Afterwards, cells were washed with PBS-T (0.05% Tween-20) and blocked with 1% BSA PBS-T for 30 min. Primary antibodies were diluted in 1% BSA PBS-T and incubated for 60 min at 37°C before the cells were washed three times with PBS-T. PLA probes PLUS (anti-rabbit) and MINUS (anti-mouse) were diluted 1:5 in 1% BSA PBS-T and incubated for another 60 min at 37°C before the Ligation and Amplification Reactions were performed as described in the PLA assay protocol. PLA signals were detected using the $\times 20$ or $\times 40$ objective of a Zeiss Imager Z1 fluorescence microscope and quantified using the 'find maxima' function of ImageJ. Cell numbers were determined from intact DAPI signal and fragmented nuclear signals resulting from dying glia cells excluded. To exclude an effect of AraC on protein interactions, PLA was performed initially on neuronal culture grown without the addition of AraC (not shown). The following antibodies were used for PLA: rabbit anti-PCLO (1:500, Synaptic Systems), mouse anti-PSD95 (1:500, Synaptic Systems), and rabbit anti-SNAP25 (1:100, Synaptic Systems).

Cell culture electrophysiology. Whole-cell patch-clamp recordings of EPSCs were obtained from 20/21 DIV neurons using a Multiclamp700A amplifier (Molecular Devices, Foster City, CA, USA) and pClamp-10 software (Axon Instruments, Foster City, CA, USA). Recordings were performed in the voltage-clamp mode. Currents were sampled at 5 kHz and filtered at 2–5 kHz. External solution (Krebs' Ringer's-HEPES (KRH)) had the following composition (in mM): 125 NaCl, 5 KCl, 1.2 MgSO_4 , 1.2 KH_2PO_4 , 2 CaCl_2 , 6 glucose, and 25 HEPES-NaOH, pH 7.4. Only cells obtained from wt and Het embryos that had resting membrane

potentials < -50 mV were considered for experiments. Resting membrane potentials were measured immediately upon breaking into whole-cell mode by setting the current to 0 pA. No differences were found between neuronal genotypes. Cells were then voltage-clamped at a holding potential of -70 mV, unless otherwise noted. Recordings of mEPSCs were obtained in the presence of Tetrodotoxin (TTX, $1 \mu\text{M}$, Tocris, Bristol, UK) to block spontaneous action potentials propagation. Recording pipettes, tip resistances of 3–5 M Ω were filled with the intracellular solution of the following composition (in mM): 130 potassium gluconate, 10 KCl, 1 EGTA, 10 HEPES, 2 MgCl₂, 4 MgATP, and 0.3 Tris-GTP. Off-line analysis of miniature events was performed by the use of Clampfit-pClamp-10 software (Molecular Devices) and events had to exceed a threshold of 10 pA to be taken into account.

For chemical LTP experiments, recordings of mEPSCs were performed using the same intracellular solution of miniature events while glycine ($100 \mu\text{M}$, Sigma-Aldrich, Milan, Italy) was applied for 3 min at room temperature in Mg²⁺-free KRH also containing TTX ($0.5 \mu\text{M}$), bicuculline ($20 \mu\text{M}$, Tocris) and strychnine ($1 \mu\text{M}$, Sigma-Aldrich).

Fluorescence recovery after photobleaching. FRAP experiments were performed by maintaining coverslips in a 37 °C heated chamber with 5% CO₂ in their own growth medium. Live imaging was performed with a confocal microscopy Leica SP5 using a HCX PL APO $\times 63/1.4$ oil objective. Photobleaching was obtained using a 488-nm laser light at 100%. Images were collected every 500 ms. The region of interest (ROI) placed over the spine was used for both photobleaching and fluorescence recovery analysis. Analysis was performed on the first 40 s of acquisition. Each image at each time point was corrected for the background and for the ongoing bleaching and normalized according to this formula: $((F_t - F_b)/(F_r - F_b))/(F_a - F_b)$, where F_t is the fluorescence of an ROI at time t , F_b is the fluorescence of the background; F_r is the fluorescence of the reference ROI at time t and F_a is the fluorescence of the ROI immediately before photobleaching. Data were fitted with a single exponential using the Leica SP5 software (Leica Microsystems) and the relative mobile fraction values have been obtained.

Statistical analysis. Statistical analysis was performed using SigmaStat 3.5 (Jandel Scientific, San Jose, CA, USA), with statistical tests used based on initial testing distribution normality. Data are presented as mean \pm S.E.M. Differences were considered to be significant if $P < 0.05$ and are indicated by an asterisk; those at $P < 0.01$ are indicated by double asterisks; those at $P < 0.001$ are indicated by triple asterisks.

Conflict of Interest

The authors declare no conflict of interest.

Acknowledgements. We wish to acknowledge Professor Reinhard Jahn (MPI, Goettingen) for his valuable suggestions. Dr Simona Rodighiero (Fondazione Filarete, Milano, Italy) for assistance with FRAP experiments, Dr Cristina Sobacchi (Istituto Clinico Humanitas, Rozzano, Italy) for helping with C57BL/6J-GFP colony and Martina Zenkner (MDC, Berlin, Germany) for technical assistance. We would like to thank the Monzino Foundation (Milano, Italy) for its generous gift of the LSM 510 Meta and Perkin Elmer Ultraview confocal microscopes. The research leading to these results has received funding from the European Union Seventh Framework Programme under grant agreement n° HEALTH-F2-2009-241498 ('EUROSPIN' project) to MM, NEZ, KR, and EW; BMBF, ERA-Net Neuron II CIPRESS to JCM; by the Italian Ministry of Health (RF-2009-1545998 to MM and RF-2009-1471694 to RB) and by PRIN 2011 and Cariplo 2011-0540 to MM, and by CNR Research Project on Aging, Regione Lombardia Project MbMM-convenzione n°18099/RCC.

Author contributions

GF designed and performed experiments and analyzed data; RM, IC, FA, DP, PT, EE, VS, ET, and AP performed experiments and analyzed data; JM PDF and provided reagents; NEZ, KR, RB, and EW discussed the data and contribute writing the paper; MM and EM designed the research and wrote the paper.

- Grant SG. Synaptopathies: diseases of the synaptome. *Curr Opin Neurobiol* 2012; **22**: 522–529.
- Sheng M, Sabatini BL, Sudhof TC. Synapses and Alzheimer's disease. *Cold Spring Harb Perspect Biol* 2012; **4**: a005777.

- Gray JA, Roth BL. Molecular targets for treating cognitive dysfunction in schizophrenia. *Schizophr Bull* 2007; **33**: 1100–1119.
- Yin DM, Chen YJ, Sathyamurthy A, Xiong WC, Mei L. Synaptic dysfunction in schizophrenia. *Adv Exp Med Biol* 2012; **970**: 493–516.
- Persico AM, Bourgeron T. Searching for ways out of the autism maze: genetic, epigenetic and environmental clues. *Trends Neurosci* 2006; **29**: 349–358.
- Pizzarelli R, Cherubini E. Alterations of GABAergic signaling in autism spectrum disorders. *Neural Plast* 2011; **2011**: 297153.
- Washbourne P, Thompson PM, Carta M, Costa ET, Mathews JR, Lopez-Bendito G et al. Genetic ablation of the t-SNARE SNAP-25 distinguishes mechanisms of neuroexocytosis. *Nat Neurosci* 2002; **5**: 19–26.
- Sudhof TC, Rothman JE. Membrane fusion: grappling with SNARE and SM proteins. *Science* 2009; **323**: 474–477.
- Pozzi D, Condliffe S, Bozzi Y, Chikhladze M, Grumelli C, Proux-Gillardeaux V et al. Activity-dependent phosphorylation of Ser187 is required for SNAP-25-negative modulation of neuronal voltage-gated calcium channels. *Proc Natl Acad Sci USA* 2008; **105**: 323–328.
- Condliffe SB, Corradini I, Pozzi D, Verderio C, Matteoli M. Endogenous SNAP-25 regulates native voltage-gated calcium channels in glutamatergic neurons. *J Biol Chem* 2010; **285**: 24968–24976.
- Feng Y, Crosbie J, Wigg K, Pathare T, Ickowicz A, Schachar R et al. The SNAP25 gene as a susceptibility gene contributing to attention-deficit hyperactivity disorder. *Mol Psychiatry* 2005; **10**: 998–1005. 973.
- Wilson MC. Coloboma mouse mutant as an animal model of hyperkinesis and attention deficit hyperactivity disorder. *Neurosci Biobehav Rev* 2000; **24**: 51–57.
- Lewis CM, Levinson DF, Wise LH, DeLisi LE, Straub RE, Hovatta I et al. Genome scan meta-analysis of schizophrenia and bipolar disorder, part II: Schizophrenia. *Am J Hum Genet* 2003; **73**: 34–48.
- Corradini I, Verderio C, Sala M, Wilson MC, Matteoli M. SNAP-25 in neuropsychiatric disorders. *Ann NY Acad Sci* 2009; **1152**: 93–99.
- Thompson PM, Egbuoma S, Vawter MP. SNAP-25 reduction in the hippocampus of patients with schizophrenia. *Prog Neuropsychopharmacol Biol Psychiatry* 2003; **27**: 411–417.
- Thompson PM, Sower AC, Perrone-Bizzozero NI. Altered levels of the synaptosomal associated protein SNAP-25 in schizophrenia. *Biol Psychiatry* 1998; **43**: 239–243.
- Hawi Z, Matthews N, Wagner J, Wallace RH, Butler TJ, Vance A et al. DNA variation in the SNAP25 gene confers risk to ADHD and is associated with reduced expression in prefrontal cortex. *PLoS ONE* 2013; **8**: e60274.
- Sharma M, Burre J, Bronk P, Zhang Y, Xu W, Sudhof TC. CSPalpha knockout causes neurodegeneration by impairing SNAP-25 function. *EMBO J* 2012; **31**: 829–841.
- Steffensen SC, Henriksen SJ, Wilson MC. Transgenic rescue of SNAP-25 restores dopamine-modulated synaptic transmission in the coloboma mutant. *Brain Res* 1999; **847**: 186–195.
- Antonucci F, Corradini I, Morini R, Fossati G, Menna E, Pozzi D et al. Reduced SNAP-25 alters short-term plasticity at developing glutamatergic synapses. *EMBO Rep* 2013; **14**: 645–651.
- Lau CG, Takayasu Y, Rodenas-Ruano A, Paternain AV, Lerma J, Bennett MV et al. SNAP-25 is a target of protein kinase C phosphorylation critical to NMDA receptor trafficking. *J Neurosci* 2010; **30**: 242–254.
- Jurado S, Goswami D, Zhang Y, Molina AJ, Sudhof TC, Malenka RC. LTP requires a unique postsynaptic SNARE fusion machinery. *Neuron* 2013; **77**: 542–558.
- Tomasoni R, Repetto D, Morini R, Elia C, Gardoni F, Di Luca M et al. SNAP-25 regulates spine formation through postsynaptic binding to p140Cap. *Nat Commun* 2013; **4**: 2136.
- Rizzi TS, Beunders G, Rizzu P, Sistermans E, Twisk JW, van Mechelen W et al. Supporting the generalist genes hypothesis for intellectual ability/disability: the case of SNAP25. *Genes Brain Behav* 2012; **11**: 767–771.
- Corradini I, Donzelli A, Antonucci F, Welz H, Loos M, Martucci R et al. Epileptiform activity and cognitive deficits in SNAP-25^{-/-} mice are normalized by antiepileptic drugs. *Cereb Cortex* 2012; **24**: 364–376.
- Kawakami S, Ohmoto M, Itoh S, Yuasa R, Inagaki H, Nishimura E et al. Accumulation of SNAP25 in mouse gustatory and somatosensory cortices in response to food and chemical stimulation. *Neuroscience* 2012; **218**: 326–334.
- Stern E, Chinnakkaruppan A, David O, Sonenberg N, Rosenblum K. Blocking the eIF2alpha kinase (PKR) enhances positive and negative forms of cortex-dependent taste memory. *J Neurosci* 2013; **33**: 2517–2525.
- Garner CC, Waites CL, Ziv NE. Synapse development: still looking for the forest, still lost in the trees. *Cell Tissue Res* 2006; **326**: 249–262.
- Okabe M, Ikawa M, Kominami K, Nakanishi T, Nishimune Y. 'Green mice' as a source of ubiquitous green cells. *FEBS Lett* 1997; **407**: 313–319.
- Lu W, Man H, Ju W, Trimble WS, MacDonald JF, Wang YT. Activation of synaptic NMDA receptors induces membrane insertion of new AMPA receptors and LTP in cultured hippocampal neurons. *Neuron* 2001; **29**: 243–254.
- Menna E, Zambetti S, Morini R, Donzelli A, Disanza A, Calvigioni D et al. Eps8 controls dendritic spine density and synaptic plasticity through its actin-capping activity. *EMBO J* 2013; **32**: 1730–1744.
- El-Husseini AE, Schnell E, Chetkovich DM, Nicoll RA, Brecht DS. PSD-95 involvement in maturation of excitatory synapses. *Science* 2000; **290**: 1364–1368.
- Sala C, Cambianica I, Rossi F. Molecular mechanisms of dendritic spine development and maintenance. *Acta Neurobiol Exp (Wars)* 2008; **68**: 289–304.

34. Grumelli C, Corradini I, Matteoli M, Verderio C. Intrinsic calcium dynamics control botulinum toxin A susceptibility in distinct neuronal populations. *Cell Calcium* 2010; **47**: 419–424.
35. Nikonenko I, Boda B, Steen S, Knott G, Welker E, Muller D. PSD-95 promotes synaptogenesis and multiinnervated spine formation through nitric oxide signaling. *J Cell Biol* 2008; **183**: 1115–1127.
36. Keller JE, Neale EA. The role of the synaptic protein snap-25 in the potency of botulinum neurotoxin type A. *J Biol Chem* 2001; **276**: 13476–13482.
37. Bresler T, Ramati Y, Zamorano PL, Zhai R, Garner CC, Ziv NE. The dynamics of SAP90/PSD-95 recruitment to new synaptic junctions. *Mol Cell Neurosci* 2001; **18**: 149–167.
38. Gray NW, Weimer RM, Bureau I, Svoboda K. Rapid redistribution of synaptic PSD-95 in the neocortex in vivo. *PLoS Biol* 2006; **4**: e370.
39. Barrios-Rodiles M, Brown KR, Ozdamar B, Bose R, Liu Z, Donovan RS *et al*. High-throughput mapping of a dynamic signaling network in mammalian cells. *Science* 2005; **307**: 1621–1625.
40. Petrakis S, Rasko T, Russ J, Friedrich RP, Stroedicke M, Riechers SP *et al*. Identification of human proteins that modify misfolding and proteotoxicity of pathogenic ataxin-1. *PLoS Genet* 2012; **8**: e1002897.
41. Jaworski J, Kapitein LC, Gouveia SM, Dortland BR, Wulf PS, Grigoriev I *et al*. Dynamic microtubules regulate dendritic spine morphology and synaptic plasticity. *Neuron* 2009; **61**: 85–100.
42. Zinkel S, Gross A, Yang E. BCL2 family in DNA damage and cell cycle control. *Cell Death Diff* 2006; **13**: 1351–1359.
43. Kasai H, Fukuda M, Watanabe S, Hayashi-Takagi A, Noguchi J. Structural dynamics of dendritic spines in memory and cognition. *Trends Neurosci* 2010; **33**: 121–129.
44. Elkobi A, Ehrlich I, Belelovsky K, Barki-Harrington L, Rosenblum K. ERK-dependent PSD-95 induction in the gustatory cortex is necessary for taste learning, but not retrieval. *Nat Neurosci* 2008; **11**: 1149–1151.
45. O'Brien RJ, Lau LF, Huganir RL. Molecular mechanisms of glutamate receptor clustering at excitatory synapses. *Curr Opin Neurobiol* 1998; **8**: 364–369.
46. Lee SH, Sheng M. Development of neuron-neuron synapses. *Curr Opin Neurobiol* 2000; **10**: 125–131.
47. Schnell E, Sizemore M, Karimzadegan S, Chen L, Bredt DS, Nicoll RA. Direct interactions between PSD-95 and stargazin control synaptic AMPA receptor number. *Proc Natl Acad Sci USA* 2002; **99**: 13902–13907.
48. Ehrlich I, Malinow R. Postsynaptic density 95 controls AMPA receptor incorporation during long-term potentiation and experience-driven synaptic plasticity. *J Neurosci* 2004; **24**: 916–927.
49. Friedman HV, Bresler T, Garner CC, Ziv NE. Assembly of new individual excitatory synapses: time course and temporal order of synaptic molecule recruitment. *Neuron* 2000; **27**: 57–69.
50. Okabe S, Miwa A, Okado H. Spine formation and correlated assembly of presynaptic and postsynaptic molecules. *J Neurosci* 2001; **21**: 6105–6114.
51. Sabo SL, Gomes RA, McAllister AK. Formation of presynaptic terminals at predefined sites along axons. *J Neurosci* 2006; **26**: 10813–10825.
52. Verhage M, Maia AS, Plomp JJ, Brussaard AB, Heeroma JH, Vermeer H *et al*. Synaptic assembly of the brain in the absence of neurotransmitter secretion. *Science* 2000; **287**: 864–869.
53. Harms KJ, Craig AM. Synapse composition and organization following chronic activity blockade in cultured hippocampal neurons. *J Comp Neurol* 2005; **490**: 72–84.
54. Bouwman J, Maia AS, Camoletto PG, Posthuma G, Roubos EW, Oorschot VM *et al*. Quantification of synapse formation and maintenance in vivo in the absence of synaptic release. *Neuroscience* 2004; **126**: 115–126.
55. McAllister AK. Dynamic aspects of CNS synapse formation. *Annu Rev Neurosci* 2007; **30**: 425–450.
56. Bronk P, Deak F, Wilson MC, Liu X, Sudhof TC, Kavalali ET. Differential effects of SNAP-25 deletion on Ca²⁺-dependent and Ca²⁺-independent neurotransmission. *J Neurophysiol* 2007; **98**: 794–806.
57. Selak S, Paternain AV, Aller MI, Pico E, Rivera R, Lerma J. A role for SNAP25 in internalization of kainate receptors and synaptic plasticity. *Neuron* 2009; **63**: 357–371.
58. Verderio C, Pozzi D, Pravettoni E, Inverardi F, Schenk U, Coco S *et al*. SNAP-25 modulation of calcium dynamics underlies differences in GABAergic and glutamatergic responsiveness to depolarization. *Neuron* 2004; **41**: 599–610.
59. Repetto D, Camera P, Melani R, Morello N, Russo I, Calcagno E *et al*. p140Cap regulates memory and synaptic plasticity through Src-mediated and Citron-N-mediated actin reorganization. *J Neurosci* 2014; **34**: 1542–1553.
60. Penzes P, Cahill ME, Jones KA, VanLeeuwen JE, Woolfrey KM. Dendritic spine pathology in neuropsychiatric disorders. *Nat Neurosci* 2011; **14**: 285–293.
61. Washbourne P, Cansino V, Mathews JR, Graham M, Burgoyne RD, Wilson MC. Cysteine residues of SNAP-25 are required for SNARE disassembly and exocytosis, but not for membrane targeting. *Biochem J* 2001; **357**: 625–634.
62. Bartlett WP, Banker GA. An electron microscopic study of the development of axons and dendrites by hippocampal neurons in culture. I. Cells which develop without intercellular contacts. *J Neurosci* 1984; **4**: 1944–1953.
63. Minerbi A, Kahana R, Goldfeld L, Kaufman M, Marom S, Ziv NE. Long-term relationships between synaptic tenacity, synaptic remodeling, and network activity. *PLoS Biol* 2009; **7**: e1000136.
64. Paxinos G, Franklin KB. *The Mouse Brain in Stereotaxic Coordinates*. Elsevier: San Diego, 2013.
65. Sala C, Piech V, Wilson NR, Passafaro M, Liu G, Sheng M. Regulation of dendritic spine morphology and synaptic function by Shank and Homer. *Neuron* 2001; **31**: 115–130.
66. Frassonni C, Inverardi F, Coco S, Ortino B, Grumelli C, Pozzi D *et al*. Analysis of SNAP-25 immunoreactivity in hippocampal inhibitory neurons during development in culture and in situ. *Neuroscience* 2005; **131**: 813–823.
67. Di Stefano P, Damiano L, Cabodi S, Aramu S, Tordella L, Praduroux A *et al*. p140Cap protein suppresses tumour cell properties, regulating Csk and Src kinase activity. *EMBO J* 2007; **26**: 2843–2855.

Supplementary Information accompanies this paper on Cell Death and Differentiation website (<http://www.nature.com/cdd>)